Prediction of Anisotropic Thermal Conductivity in Short Carbon Fiber Reinforced Polymers using Multiscale Analysis

Harry H. Zhou[1]*, and Sergii G. Kravchenko[1]

[1] Department of Materials Engineering, The University of British Columbia, Vancouver, Canada

* *Corresponding author (harry.zhou@ubc.ca)*

Keywords: *Finite Element Modelling; Thermal Conductivity; Microstructural Characterization; Anisotropy*

Abstract

Reliable thermal management in composite materials depends on knowledge of their thermal conductivity, which governs heat dissipation and temperature evolution. Most experimental techniques for measuring thermal conductivity rely on isotropic regression models, making them unsuitable for anisotropic composites. The Transient Plane Source method uniquely allows for the determination of transversely isotropic thermal conductivity when measurements are aligned with principal directions. To address this, a computational-experimental framework is presented for the prediction of anisotropic thermal conductivity through computational homogenization based on experimentally extracted microstructural characteristics. Micro-computed tomography characterizes the microstructure of a short carbon fiber reinforced polyetherimide composite fabricated via Fused Filament Fabrication. Extracted statistics, such as fiber and void geometry, volume fraction, and spatial distribution, inform the generation of representative volume elements, which are analyzed through micromechanical modeling to determine the thermal conductivity tensor. A finite element model of the Transient Plane Source method is developed to simulate the transient temperature change using the predicted tensor. Comparison between simulated and experimental thermal response is performed in multiple directions, enabling quantitative validation of predicted anisotropic thermal conductivity. The proposed framework enables prediction of thermal conductivity in short carbon fiber composites without relying on symmetry assumptions, providing a generalized approach for anisotropic thermal characterization.

1. Introduction

Understanding the thermal conductivity (TC) of composite materials is essential for thermal management applications. However, accurate measurement of TC in anisotropic materials, such as short carbon fiber–reinforced polymers (SCFRP), remains challenging. Unlike isotropic materials characterized by a single scalar value, anisotropic materials exhibit direction-dependent thermal transport and are described by a second-order TC tensor with distinct principal values and orientations. Conventional TC measurement techniques, including transient plane source (TPS), heat flow meters, and laser flash analysis [1], [2], rely on analytical solutions that assume isotropic behavior. Among these, the TPS method can measure transversely isotropic TC [3]; however, it requires prior knowledge of the principal conduction directions, which is often unavailable in practice. Consequently, applying these methods to fully anisotropic materials yields configurationdependent results that do not represent intrinsic material properties. As such, no direct experimental approach currently exists to determine the full anisotropic TC tensor of heterogeneous materials without a priori assumptions regarding symmetry.

The anisotropic thermal behavior of SCFRP arises from the morphology, volume fraction, and spatial distribution of its constituent phases [4], [5], [6], [7]. In melt-extrusion additive manufacturing, processing conditions significantly influence microstructural statistics. For instance, fibers tend to align along the printing direction due to shear-induced effects, forming conductive pathways that enhance heat transfer [6]. Conversely, elongated voids aligned with the heat flux direction can significantly disrupt thermal transport compared to more equiaxed voids [7]. The combined influence of fiber and void characteristics governs the overall TC and directional heat conduction behavior of SCFRP.

Computational homogenization provides a multiscale framework for predicting effective material properties of materials with complex microstructures[8], [9]. Representative Volume Elements (RVEs) that capture the statistical features of heterogeneous materials are subjected to thermal loading, and their averaged response is used to determine effective properties. For example, Tian et al. [8] employed finite element (FE) simulations of steady-state heat transfer in RVEs and applied Fourier's law to extract the effective TC tensor.

Despite the effectiveness of such computational approaches, validation remains a key challenge. Direct comparison between predicted and experimentally measured TC values is insufficient for fully anisotropic materials, as conventional measurement techniques cannot resolve the complete TC tensor. Numerical models of the TPS method have been used to evaluate measurement accuracy under varying conditions[10], [11]. These models are typically validated against transient temperature–time responses using experimentally measured thermal properties.

In this work, a microstructure-informed framework is developed to predict the full TC tensor which is then validated against experimentally measured TPS temperature–time curves. A short carbon fiber polyetherimide (SCF/PEI) specimen was fabricated via melt-extrusion additive manufacturing, and its microstructural characteristics, including fiber orientation tensors, volume fractions, and phase morphologies were quantified using microcomputed tomography (μCT) imaging. A statistically representative RVE was generated in Digimat, and FE heat transfer simulations were performed to compute the effective TC tensor. The predicted tensor was subsequently used as input for TPS simulations replicating the experimental configuration. Simulated and measured temperature-time responses were compared across multiple reference directions, enabling a rigorous assessment of the predictive capability of the model.

2. Materials and Methods

2.1. Sample Preparation

Fused Filament Fabrication (FFF) was used to print unidirectional 20×20×20mm cubes for TPS experiments, and single bead samples were prepared for μCT imaging. The samples were printed using the AON3D M2+ printer, and Table 1 lists the printing parameters used.

Table 1: Printing Parameters used for Sample Fabrication

Printing Parameter	
Bed temperature (°C)	175
Chamber temperature (°C)	135
Nozzle Temperature (°C)	365

Nozzle Size (mm)	0.6
Bead Width, W (mm)	0.65
Layer Height, H (mm)	0.3
Print Speed (mm/s)	40.0

This paper presents TPS transient temperature curves in multiple reference directions, x_1, x_2, and x_3. These directions are chosen based on the unidirectional deposition during the printing process, with x_1 along the printing direction, x_2 along the transverse direction, parallel to the slice plane, and x_3 in the build direction.

2.2. Microstructural Characterization

Microstructural characteristics that were used in this study were obtained by Ke et al. [4]. The microstructural characteristics were obtained using Zeiss Xradia 520 Versa µCT system. The 2D projections of a 2×2×2mm volume was captured, as it rotated 360º. The resolution used was 3µm, with a voltage of 40kV, power of 5W for a total of 3201 projections, each with an exposure of 0.5 seconds. XMReconstructor was used for tomographic reconstruction, which results in an image stack which can be imported into VGStudio Max 2024.1 for analysis.

2.3. Representative Volume Element Generation

RVE generation was performed using Digimat-FE 2025.1. Table 2 lists the fiber and void characteristics used as reference values for the generation process. The RVE size was set to 300 × 250 × 250 µm, to allow for the volume fractions and orientations to be approximated. The RVE was then meshed with a element seed size of 3µm, and minimum element size of 0.7µm, to ensure small microstructural details could be meshes properly. The initial seed size of 3µm was chosen to ensure at least 2 elements across the diameter of each fiber. Periodic boundary conditions were applied, and the mesh was subsequently exported as an ABAQUS input file for simulation.

Table 2: Microstructural Parameters used for Representative Volume Element Generation

Fiber/ Void Orientation Tensor	$\begin{bmatrix} 0.79 & -0.01 & 0.01 \\ \vdots & 0.11 & 0 \\ \text{symm} & \cdots & 0.1 \end{bmatrix}$
Fiber Shape	Sphero-cylindrical
Fiber Diameter (µm)	7
Fiber Length (µm)	67
Fiber Volume Fraction	0.08
Void Shape	Ellipsoid
Void Diameter (µm)	17
Void Length (µm)	25
Void Volume Fraction	0.24

The constituent material properties used in the RVE can be found below, in Table 3.

Table 3: Constituent Material Properties [4]

	Carbon Fiber	PEI	Air
Thermal conductivity $\left({}^{W}/_{mK}\right)$	$\begin{bmatrix} 6.83 & & \\ & 2.18 & \\ & & 2.18 \end{bmatrix}$	0.22	0.03
Density $\left({}^{kg}/_{m^3}\right)$	1790	1270	1.23
Specific Heat $\left({}^{J}/_{kgK}\right)$	1258	1134	1005

2.4. Computational Homogenization Scheme

This work applies a computational homogenization scheme presented by Tian et al. The generated RVEs were utilized in a steady-state thermal analysis using ABAQUS 2022. Three simulations were performed, and each simulation had prescribed temperature differences between parallel faces, $T^{\text{RP-1}}$, $T^{\text{RP-2}}$ and $T^{\text{RP-3}}$. Figure 1(a) depicts each pair of faces, as well as the For each simulation, a prescribed temperature change was set to 144°K, while the other two were set to 0°K. Eq. (1) can then be used to determine the heat flux tensor $\langle q \rangle_i$

$$q_i = \frac{1}{V_{\text{RVE}}} \sum_e V_e \left(\sum_{I=1}^{n_e} q_i(y_I) W(y_I) \right), \tag{1}$$

where n_e is the number of integration points in the element e, $q_i(y_I)$, and $W(y_I)$ are the heat flux and weight of the integration point, respectively, and V_{RVE} and V_e are the volumes of the RVE and element, respectively. With $i = 1,2,$ and 3, the heat flux tensor can be used to calculate the effective TC tensor, as shown in Eq. (2).

$$k_{ij} = {}^{-q_i}/_{\nabla T_j}, \tag{2}$$

where $\nabla T_j = {}^{\Delta T_j}/_{L_j}$, ΔT_j and L_j is the difference in temperature between two opposite sides of an RVE normal to the x_j axis, and the length of the RVE in the x_j direction, respectively.

2.5. Validation

Validation was performed by simulating the TPS experiment using the predicted TC and comparing the resulting temperature vs. time curves against experimentally measured curves. This study uses experimental temperature-time curves obtained by Ke et al. [4]. Table 4 describes the TPS experimental parameters used.

Table 4: Experimental Parameters used for Transient Plane Source Method

	x_1	x_2	x_3
Heating Power (mW)	15	15	15
Heating Time (s)	20	20	20

Figure 1 depicts the model reduction steps, Figure 1 (a) shows the experimental TPS setup, and Figure 1 (b) shows the TPS model reduced along the planes of symmetry. The sample was modelled as 10 × 10 × 10 mm block, and the sensor was modelled as an extruded quarter-circle with a radius of 3.19 mm and a thickness of 0.07 mm. The sample length in the x_k direction was reduced after initial test runs showed that the semi-infinite medium assumption for TPS was satisfied with the shorter length. A simple surface contact constraint was applied to the sensor/ sample interface, and a large thermal conductance was applied to model perfect contact (i.e. no thermal resistance at the interface). All external faces and symmetry planes had adiabatic boundary conditions prescribed. The TPS sensor was not explicitly modelled; only the Kapton insulating layer was modelled, and a surface heat flux was applied to its outer surface [11].

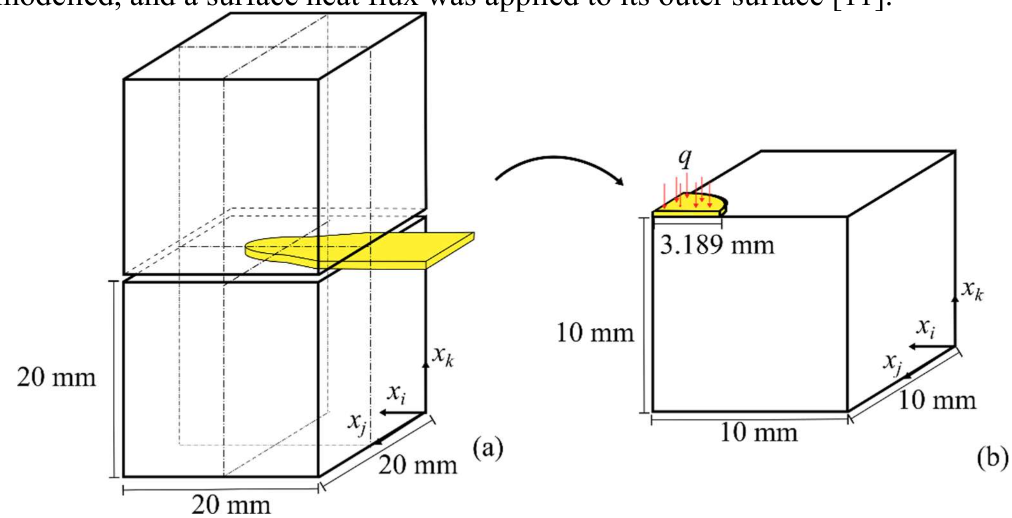

Figure 1: Schematic of (a) the Transient Plane Source Method, and (b) the Simplified Model used for Finite Element Analysis

Simulated temperature-time curves were obtained in all three reference directions (x_1, x_2, x_3) using the predicted thermal conductivity tensor. The volume-averaged temperature of all elements in the sensor was used as the temperature at each time increment. Table 5 shows the known material properties of the sample and sensor. The specific heat and density of the sample were calculated using the rule of mixtures.

Table 5: Sample and Sensor Material Properties used for Validation

	Sample	Sensor
Thermal conductivity ($^{W}/_{mK}$)	--	0.2
Density ($^{kg}/_{m^3}$)	1019	1420
Specific Heat ($^{J}/_{kgK}$)	1189	1100

Additionally, the TPS FEA model is performed by comparing experimental and simulated temperature vs. time curves by utilizing experimentally measured thermal properties, which are listed in Table 6. Three comparisons were made, one for each reference direction. The specific heat for simulations performed in the x_2 and x_3 directions are products of the regression method use, but is treated as an effective parameter to fit experimental TPS curves, which is acceptable for validating the TPS FE model response in those directions.

Table 6: Thermal Properties of the Sample Material used to Validate the Finite Element Model

	x_1	x_2	x_3
Thermal Conductivity ($\times 10^{-1}\,\mathrm{W}/_{\mathrm{mK}}$)	$\begin{bmatrix} 2.6 & & \\ & 2.0 & \\ & & 2.0 \end{bmatrix}$	2.3	2.1
Specific Heat ($\mathrm{J}/_{\mathrm{kgK}}$)	1010	886	525
Density ($\mathrm{kg}/_{\mathrm{m^3}}$)	1019		

3. Results and Discussion

3.1. Representative Volume Element Generation

Figure 2b depicts the microstructure of the RVE generated in Section 2.3 and for qualitative comparison, Figure 2a depicts the microstructure captured from μCT. It can be seen in both microstructures, the fibers align preferentially in the x_1 direction, and fibers penetrating voids. The fiber and void volume fractions were 0.08, and 0.24.

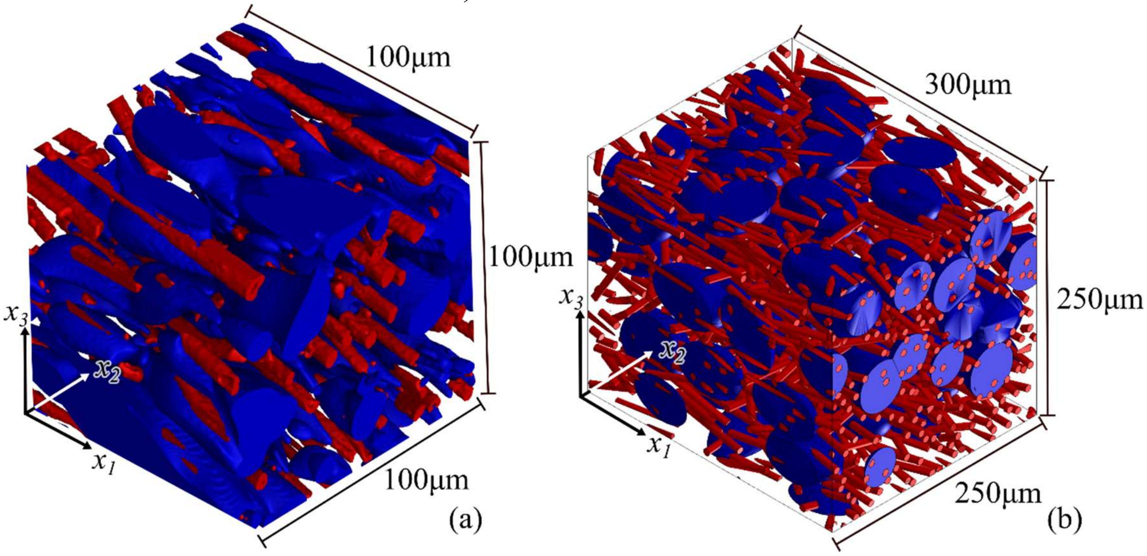

Figure 2: (a) Example volume of FFF microstructure measured using μCT and (b) Representative Volume Element of FFF microstructure

The fiber and void orientation tensors are shown below. The global error for fiber and void orientation were 0.051 and 0.054, respectively.

$$a_{ij}^{\text{fiber}} = \begin{bmatrix} 0.81 & -0.0069 & 0.0017 \\ \vdots & 0.125 & -0.0049 \\ \text{symm} & \cdots & 0.061 \end{bmatrix}, a_{ij}^{\text{void}} = \begin{bmatrix} 0.82 & -0.0152 & 0.025 \\ \vdots & 0.087 & 0.019 \\ \text{symm} & \cdots & 0.090 \end{bmatrix}.$$

Due to the random placement of fiber and voids into the RVE and the finite domain of the RVE, reaching the reference volume fraction and orientation state can be challenging. However, the above RVE is acceptable for this initial application. A more exhaustive study could perform size convergence or ensemble averaging over multiple RVEs, which is left for future work.

3.2. Thermal Conductivity Prediction

The predicted thermal conductivity tensor, k_{ij}^{sim}, can be seen below. The tensor closely resembles transverse isotropy, with k_{11}^{sim} larger then k_{22}^{sim} and k_{33}^{sim}. This is expected, as the fiber and void orientation both exhibited preferential alignment with the x_1 direction, and similar alignment in the radial directions.

$$k_{ij}^{\text{sim}} = \begin{bmatrix} 2.41\times10^{-1} & 3.23\times10^{-4} & 1.28\times10^{-3} \\ 4.48\times10^{-4} & 1.61\times10^{-1} & 2.52\times10^{-3} \\ 1.88\times10^{-3} & 2.54\times10^{-3} & 1.53\times10^{-1} \end{bmatrix} \mathrm{W}/_{\mathrm{mK}}$$

3.3. Transient Plane Source Method Model Validation

Figure 3 shows the simulated temperature-time curves obtained in the x_1, x_2 and x_3 directions using thermal properties obtained experimentally. Before comparison was performed, the simulated curves were shifted vertically to align with experimentally measured curves. This temperature shift is present due to assumptions made in the FE model, such as the lack of interfacial thermal contact resistance and sensor model simplifications. To account for this, the average temperature difference between experimental and simulated curves was determined and was sued to shift the simulated temperature. The first 20 data points in both experimental and simulated datasets were ignored during this process. All comparisons of the temperature vs. time curves are performed after this temperature shift.

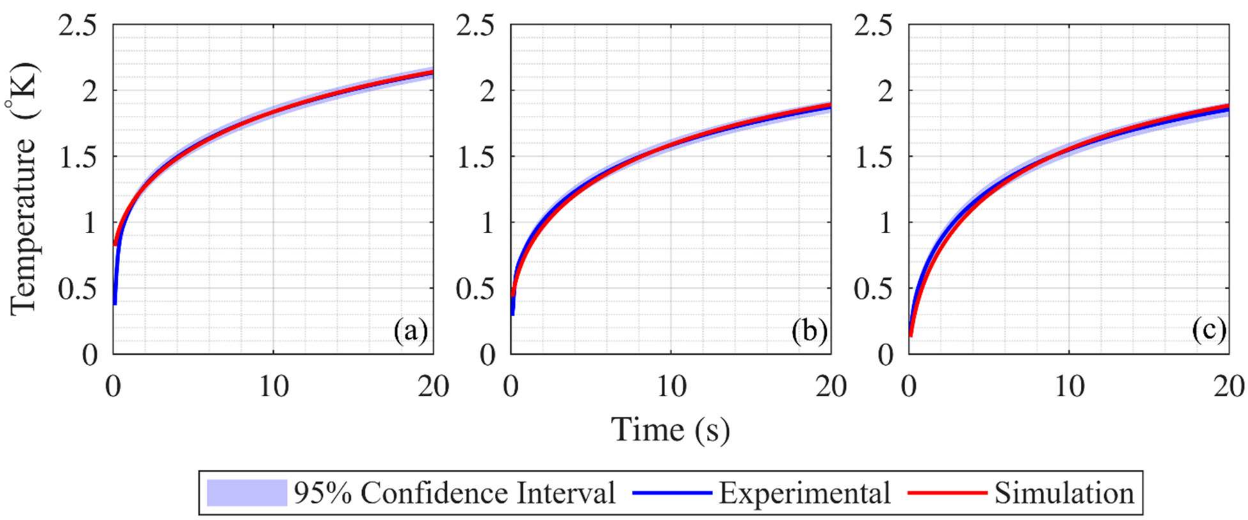

Figure 3: Comparison of Experimental and Simulated TPS Method using Experimentally Measured Thermal Conductivity in the (a) x_1, (b) x_2 and (c) x_3 Directions

The average and maximum deviation between the two are listed in Table 7. From these results, it can be seen that the FE model is able to reproduce the experimental results with strong alignment. The highest deviation can be seen in the x_3 direction, with an average of 1.67% and maximum of 7.94%. The x_1 direction showed the strongest alignment, with an average deviation of 0.27% and maximum of 0.68.

Table 7: Mean and Max Error Between Experimental and Simulated Temperature vs. Time using Experimentally Measured Thermal Properties

	Average Error (%)	Maximum Error (%)
x_1	0.27	0.68
x_2	1.02	4.29
x_3	1.67	7.94

3.4. Prediction Validation

Figure 4 depicts the experimental and simulated temperature vs. time curves, using the predicted thermal conductivity.

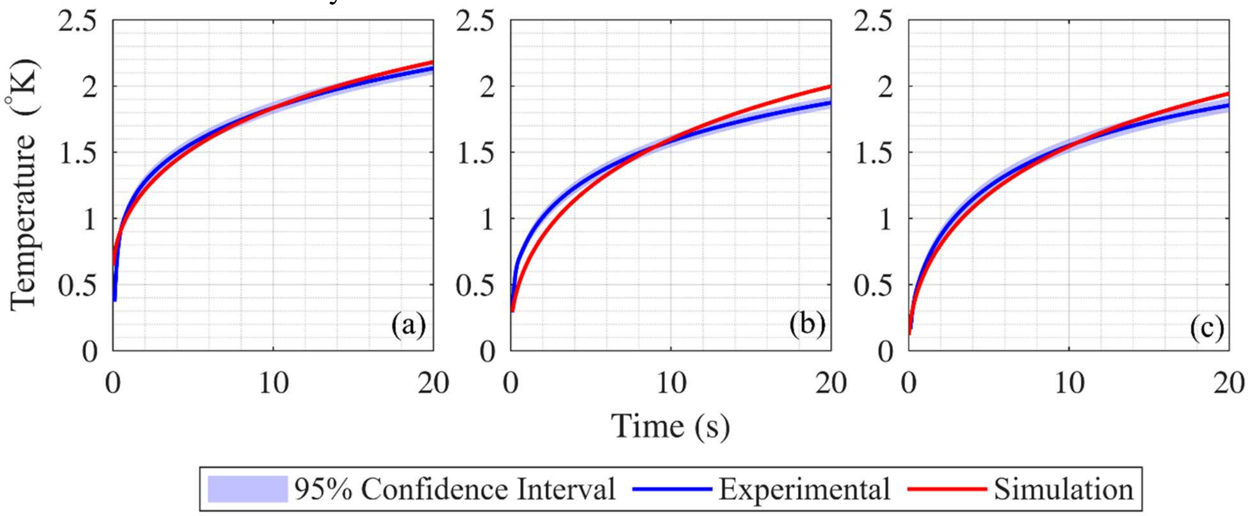

Figure 4: Comparison of Experimental and Simulated TPS Method using Predicted Thermal Conductivity in the (a) x_1, (b) x_2 and (c) x_3 Directions

Table 8 lists the average and maximum deviations between the two methods. The largest deviation can be seen in the x_2 direction, with an average deviation of 4.44, and maximum of 15.84%. x_1 shows the strongest alignment with an average deviation of 1.64% and maximum of 4.83%. This could be due to deviations from the reference fiber and void orientation, during the RVE generation process. The higher deviations in the x_2 and x_3 directions could also be due to the relationship between the fiber and void orientation in those directions. Both the fiber and void orientation tensors deviated from the reference values, and in opposite directions, leading to large differences in alignment in those directions.

Table 8: Mean and Max Error Between Experimental and Simulated Temperature vs. Time using Predicted Thermal Conductivity

	Average Error (%)	Maximum Error (%)
x_1	1.64	4.83
x_2	4.44	15.84
x_3	3.12	8.31

It should also be noted that the inherent error is included in the observed error. For example, deviation in the reference direction x_3 when validating the TPS model was 1.67, which is around half of the error reported when using the predicted thermal conductivity.

4. Conclusion

This study presents a methodology for predicting the full TC tensor without imposing assumptions on material symmetry. The predicted TC tensor was implemented within a TPS FE model, and the resulting temperature–time responses were compared against experimental measurements. The predicted thermal conductivities show reasonably good agreement with experimentally obtained values, with average deviations below 5% in all directions and higher maximum deviations in the transverse directions.

Potential improvements include enhanced control over fiber and void alignment relative to reference parameters, as well as refinement of the TPS FE model to better capture interfacial contact physics. Overall, the results indicate that the proposed approach effectively captures the thermal behavior of the material without requiring prior assumptions regarding symmetry planes. These results demonstrate that the framework can capture the primary anisotropic features of the thermal response and provide a practical route to estimating anisotropic TC tensors.

References

[1] S. E. Gustafsson, “Transient plane source techniques for thermal conductivity and thermal diffusivity measurements of solid materials,” *Rev. Sci. Instrum.*, vol. 62, no. 3, pp. 797–804, Mar. 1991, doi: 10.1063/1.1142087.

[2] W. J. Parker, R. J. Jenkins, C. P. Butler, and G. L. Abbott, “Flash Method of Determining Thermal Diffusivity, Heat Capacity, and Thermal Conductivity,” *J. Appl. Phys.*, vol. 32, no. 9, pp. 1679–1684, Sep. 1961, doi: 10.1063/1.1728417.

[3] S. Gustafsson, “On the Development of the Hot Strip, Hot Disc, and Pulse Hot Strip Methods for Measuring Thermal Transport Properties,” *Int. Therm. Conduct. Conf. ITCC Int. Therm. Expans. Symp. ITES*, p. 3, Oct. 2015.

[4] T. Ke *et al.*, “Microstructure Statistical Symmetry, and Quantification of Anisotropic Thermal Conduction in Additive Manufactured Short Carbon Fiber/Polyetherimide Composites,” *J. Manuf. Mater. Process.*, vol. 10, no. 1, Dec. 2025, doi: 10.3390/jmmp10010016.

[5] H. Gonabadi, S. F. Hosseini, Y. Chen, and S. Bull, “Size effects of voids on the mechanical properties of 3D printed parts,” *Int. J. Adv. Manuf. Technol.*, vol. 132, no. 11–12, pp. 5439–5456, Jun. 2024, doi: 10.1007/S00170-024-13683-9/TABLES/7.

[6] Z. Wang, Z. Fang, Z. Xie, and D. E. Smith, “A Review on Microstructural Formations of Discontinuous Fiber-Reinforced Polymer Composites Prepared via Material Extrusion Additive Manufacturing: Fiber Orientation, Fiber Attrition, and Micro-Voids Distribution,” *Polymers*, vol. 14, no. 22, p. 4941, Jan. 2022, doi: 10.3390/polym14224941.

[7] Y. Tao *et al.*, “A review on voids of 3D printed parts by fused filament fabrication,” *J. Mater. Res. Technol.*, vol. 15, pp. 4860–4879, Nov. 2021, doi: 10.1016/J.JMRT.2021.10.108.

[8] W. Tian, L. Qi, X. Chao, J. Liang, and M. W. Fu, “Numerical evaluation on the effective thermal conductivity of the composites with discontinuous inclusions: Periodic boundary condition and its numerical algorithm,” *Int. J. Heat Mass Transf.*, vol. 134, pp. 735–751, May 2019, doi: 10.1016/j.ijheatmasstransfer.2019.01.072.

[9] I. Özdemir, W. A. M. Brekelmans, and M. G. D. Geers, “Computational homogenization for heat conduction in heterogeneous solids,” *Int. J. Numer. Methods Eng.*, vol. 73, no. 2, pp. 185–204, Jan. 2008, doi: 10.1002/nme.2068.

[10] H. Zhang, Y. Jin, W. Gu, Z. Y. Li, and W. Q. Tao, “A numerical study on the influence of insulating layer of the hot disk sensor on the thermal conductivity measuring accuracy,” *Prog. Comput. Fluid Dyn. Int. J.*, vol. 13, no. 3/4, p. 191, 2013, doi: 10.1504/PCFD.2013.053660.

[11] S. Tarasovs and A. Aniskevich, “Identification of the anisotropic thermal conductivity by an inverse solution using the transient plane source method,” *Measurement*, vol. 206, p. 112252, Jan. 2023, doi: 10.1016/j.measurement.2022.112252.